INTERNATIONAL CENTER FOR NUMERICAL METHODS IN ENGINEERING

Arbitrary Lagrangian-Eulerian Formulation for Fluid-Rigid Body Interaction

J. Sarrate
A. Huerta
J. Donea

Publication CIMNE Nº-137, September 1998

ARBITRARY LAGRANGIAN-EULERIAN FORMULATION FOR FLUID–RIGID BODY INTERACTION [1]

Josep Sarrate, Antonio Huerta

Departament de Matemàtica Aplicada III
E.T.S. Ingenieros de Caminos
Universitat Politècnica de Catalunya
E-08034 Barcelona, SPAIN

Jean Donea

Aerospace Laboratory-Thermomechanics
University of Liège
rue E. Solvay, 21,
B-4000 Liège, BELGIUM

Abstract

A new formulation for two–dimensional fluid–rigid body interaction problems is developed. In particular, vortex–induced oscillations of a rigid body in viscous incompressible flow are studied. The incompressible Navier–Stokes equations are used to describe the motion of the fluid, while it is assumed that the rigid body is mounted on a system consisting of a spring and a dashpot. An arbitrary Lagrangian–Eulerian formulation (ALE) is used in order to account for large boundary motion. A general formulation for the coupled problem is obtained by uncoupling the translation motion of the body from its rotational motion and developing a specific algorithm to efficiently handle the nonlinear dependence of the rotations. This general formulation can be easily applied to multi–body problems. Two numerical examples involving either translations and rotations are presented as an illustration of the proposed methodologies for fluid–rigid body interaction.

Key words: Fluid-structure interaction, arbitrary Lagrangian-Eulerian formulation, vortex shedding, induced oscillations, large boundary motion, transient Navier-Stokes

[1] This work was partially sponsored by the DGICYT of the Spanish Government (under grant PB94-1200) and by the Commission of the European Communities (under grant ERB-4050-PL-94-1116).

1 INTRODUCTION

Over the last decades, technological development in several engineering fields has placed emphasis on fluid-structure interaction [1,3,5,7,9,10]. As a consequence, numerical simulation of coupled hydrodynamic/structural problems has become one of the most challenging problems in computational fluid dynamics. In some circumstances, especially when the structure is embedded in a fluid and its deformations are small compared to the displacements and rotations of its center of gravity, it is justified to idealize the structure as a rigid body resting on an system consisting of springs and dashpots. Typical situations in which such an idealisation is legitimate include the simulation of wind-induced vibrations in high-rise buildings or large bridge girders, the cyclic response of offshore structures exposed to sea currents, as well as the behaviour of structures in aeronautical and naval engineering where structural loading and response are dominated by fluid induced vibrations.

In most cases, oscillations are due to a vortex shedding process around a structure that can be considered as a rigid body. As vortices are shed, the pressure distribution on the body is modified and time-dependent dynamic forces appear, hence inducing structural vibrations. The rigid body motion interferes with the flow pattern through a nonlinear interactive process and it is possible that, for a specific range of Reynolds numbers, the shedding frequency becomes close to one of the natural frequencies of the immersed body. In these cases, resonance occurs, both frequencies collapse to the same value and the rigid body motion, as well as the dynamic forces can become very large. This phenomenon, known as *lock–in*, can be critical for the structural design, because the flow induced dynamic forces have a direct influence on the possible catastrophic failure of the structure under consideration. It is, therefore, of prime importance from the viewpoint of structural safety to determine in which range of Reynolds numbers resonance can appear and to appraise the ensuing oscillation amplitude.

In the numerical simulation of fluid–structure interaction, see for instance [6,7,9,11–14], one of the most critical issues is the treatment of the nonlinear convective terms in the Navier–Stokes equations governing the fluid motion. However, when considering vortex induced oscillations of rigid bodies, the situation is further complicated due to the appearance of two geometric non linearities. The first one arises from the explicit dependence of the governing equations on the rotation angle of the rigid body. The second is related to the interface between the fluid and the solid domains. The interface is part of the boundary of the fluid domain, its position is unknown *a priori*, and its motion may be relatively large. Thus, its location is governed by the incompressible Navier-Stokes equations with large boundary motion, the rigid body equilibrium equations, and the restrictions imposed by the fact that the structure is

rigid.

To solve the first problem, we introduce in the present paper a new algorithm that allows to analyze the fluid–rigid body interaction problem by uncoupling the translation part of the rigid body motion from its rotational part. We also develop a specific algorithm, based on Sherman and Morrison lemma [4], to handle properly the nonlinear dependence of the rotations. For solving the second problem above, we propose using the arbitrary Lagrangian–Eulerian (ALE) formulation [5,7,9]. It allows to combine the ease of a Lagrangian description for treating the solid surface and for enforcing the compatibility and equilibrium conditions between the fluid and the rigid body. And, at the same time, it exploits the superiority of an Eulerian description for dealing with the possible distortions of the hydrodynamic domain far away from the moving boundaries. Furthermore, the freedom offered by the ALE description to move the mesh of nodal points independently of the material particles represents an easy way of adapting the fluid mesh in response to the solid movement.

The outline of the remainder of the paper is as follows. In Section 2 we introduce the problem statement by describing the equations governing the transient motion of the fluid and of the embedded rigid body. Then, we specify the compatibility conditions at the fluid/structure interface and briefly discuss the algorithm used for displacing the mesh points in the ALE domain. In Section 3 we develop a new algorithm to properly handle the nonlinearities due to explicit dependence of the flow equations on the rotation angle of the immersed rigid body. Finally, in Section 4, we present and discuss our numerical results.

2 PROBLEM STATEMENT

2.1 Fluid motion equations

Consider a two–dimensional rigid body immersed in an incompressible fluid. The motion of the fluid is governed by the incompressible Navier-Stokes equations which are given as follows in the ALE description:

$$\frac{\partial \mathbf{v}}{\partial t} + (\mathbf{v} - \hat{\mathbf{v}}) \cdot \nabla \mathbf{v} = -\nabla p + \nu \nabla^2 \mathbf{v} + \boldsymbol{f}_b,$$
$$\nabla \cdot \mathbf{v} = 0,$$

where $\mathbf{v}$ is the fluid velocity, $\hat{\mathbf{v}}$ the fluid mesh velocity, p is the fluid pressure divided by the density, ν is the kinematic viscosity, and $\boldsymbol{f}_b$ represent body forces. Appropriate initial and boundary conditions are assumed to be given.

After spatial discretization by the finite element method, the unsteady Navier–Stokes equations describing the motion of a viscous incompressible fluid are expressed as follows in the ALE formulation [7]:

$$\boldsymbol{M}\boldsymbol{a} + \boldsymbol{\eta}(\boldsymbol{v} - \hat{\boldsymbol{v}}) + \boldsymbol{K}_\mu \boldsymbol{v} - \boldsymbol{G}\boldsymbol{p} = \boldsymbol{f}, \tag{1}$$

$$\boldsymbol{G}^T \boldsymbol{v} = \boldsymbol{0}, \tag{2}$$

where $\boldsymbol{M}$ is the mass matrix; $\boldsymbol{\eta}$ represents the nonlinear convective terms depending on the relative velocity $\boldsymbol{v} - \hat{\boldsymbol{v}}$ between fluid velocity and mesh velocity; $\boldsymbol{K}_\mu$ is the fluid viscosity matrix; $\boldsymbol{G}$ is the gradient matrix and $\boldsymbol{G}^T$ the divergence matrix; $\boldsymbol{f}$ is the global vector of external loads applied on the fluid; $\boldsymbol{v}$, $\boldsymbol{a}$ and $\boldsymbol{p}$ are global vectors listing the nodal values of velocity, acceleration and pressure, respectively; finally, $\hat{\boldsymbol{v}}$ is the global nodal vector listing the components of the fluid mesh velocity.

Vectors $\boldsymbol{a}$, $\boldsymbol{v}$ and $\boldsymbol{f}$ are decomposed in a similar manner to [14],

$$\boldsymbol{a}^T = \left\{\boldsymbol{a}^f, \boldsymbol{a}^s, \tilde{\boldsymbol{a}}^d\right\} \qquad \boldsymbol{v}^T = \left\{\boldsymbol{v}^f, \boldsymbol{v}^s, \tilde{\boldsymbol{v}}^d\right\} \qquad \boldsymbol{f}^T = \left\{\tilde{\boldsymbol{f}}^f, \boldsymbol{f}^s, \boldsymbol{f}^d\right\},$$

where superscript $(^f)$ indicates values related to nodes placed in the fluid or on the Neumann portion of the boundary, superscript $(^s)$ means values related to fluid nodes on the rigid body surface, superscript $(^d)$ indicates values related to nodes on the Dirichlet portion of the boundary and the tilde symbol $(\tilde{\ })$ denotes prescribed values. According to this decomposition, the momentum conservation equation (1) can be rewritten as

$$\begin{pmatrix} \boldsymbol{M}^{ff} & \boldsymbol{M}^{fs} & \boldsymbol{M}^{fd} \\ \boldsymbol{M}^{sf} & \boldsymbol{M}^{ss} & \boldsymbol{M}^{sd} \\ \boldsymbol{M}^{df} & \boldsymbol{M}^{ds} & \boldsymbol{M}^{dd} \end{pmatrix} \begin{Bmatrix} \boldsymbol{a}^f \\ \boldsymbol{a}^s \\ \tilde{\boldsymbol{a}}^d \end{Bmatrix} + \begin{pmatrix} \boldsymbol{K}^{ff} & \boldsymbol{K}^{fs} & \boldsymbol{K}^{fd} \\ \boldsymbol{K}^{sf} & \boldsymbol{K}^{ss} & \boldsymbol{K}^{sd} \\ \boldsymbol{K}^{df} & \boldsymbol{K}^{ds} & \boldsymbol{K}^{dd} \end{pmatrix} \begin{Bmatrix} \boldsymbol{v}^f \\ \boldsymbol{v}^s \\ \tilde{\boldsymbol{v}}^d \end{Bmatrix} + \begin{Bmatrix} \boldsymbol{\eta}^f \\ \boldsymbol{\eta}^s \\ \boldsymbol{\eta}^d \end{Bmatrix} - \begin{pmatrix} \boldsymbol{G}^f \\ \boldsymbol{G}^s \\ \boldsymbol{G}^d \end{pmatrix} \boldsymbol{P} = \begin{Bmatrix} \tilde{\boldsymbol{f}}^f \\ \boldsymbol{f}^s \\ \boldsymbol{f}^d \end{Bmatrix}, \tag{3}$$

while the mass conservation equation (2) takes the following form

$$\begin{pmatrix} \boldsymbol{G}^{f^T} & \boldsymbol{G}^{s^T} & \boldsymbol{G}^{d^T} \end{pmatrix} \begin{Bmatrix} \boldsymbol{v}^f \\ \boldsymbol{v}^s \\ \tilde{\boldsymbol{v}}^d \end{Bmatrix} = \boldsymbol{0}. \tag{4}$$

Equation (3) clearly shows that the coupling between the fluid and the rigid body has to be achieved through variables defined on the rigid body surface, namely: $\boldsymbol{a}^s$, $\boldsymbol{v}^s$ and $\boldsymbol{f}^s$.

In the two–dimensional case, the motion of the rigid body has three degrees of freedom defined at the center of gravity of the body: two translational displacements, δ_1 and δ_2, and one rotational displacement, θ. The rigid body is assumed to be mounted on a system composed of elastic springs and dashpots (see Fig. 1) and its equation of motion is given by

$$\boldsymbol{\mathcal{M}}\boldsymbol{\alpha} + \boldsymbol{\mathcal{C}}\boldsymbol{\nu} + \boldsymbol{\mathcal{K}}\boldsymbol{\delta} = \boldsymbol{\varphi} \tag{5}$$

where $\boldsymbol{\mathcal{M}}$, $\boldsymbol{\mathcal{C}}$ and $\boldsymbol{\mathcal{K}}$ are the mass, damping and stiffness matrices, respectively. If each individual system is uncoupled from the others, the above matrices are diagonal and possess constant coefficients. For the subsequent developments, we also define the following vectors (see Fig. 1):

$$\boldsymbol{\delta}^T = \{\delta_1, \delta_2, \theta\} \quad \boldsymbol{\nu}^T = \{\dot{\delta}_1, \dot{\delta}_2, \dot{\theta}\} \quad \boldsymbol{\alpha}^T = \{\ddot{\delta}_1, \ddot{\delta}_2, \ddot{\theta}\} \quad \boldsymbol{\varphi}^T = \{\varphi_1, \varphi_2, \varphi_3\}$$

where $\boldsymbol{\delta}$, $\boldsymbol{\nu}$ and $\boldsymbol{\alpha}$ are the center of gravity displacement, velocity and acceleration, while $\boldsymbol{\varphi}$ contains the force and the momentum resultants. In particular cases, some of the above degrees of freedom are fixed and system (5) is therefore reduced to one or two equations for the remaining degrees of freedom.

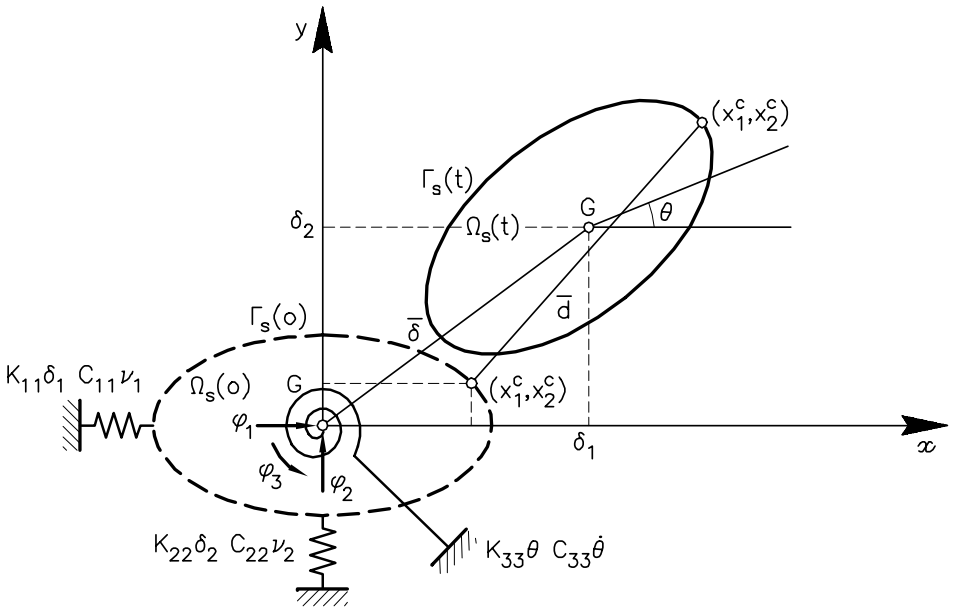

Fig. 1. Two–dimensional rigid body model

Compatibility equations are developed in order to relate variables defined at the center of gravity of the rigid body with those defined on its surface, see [14,15] for details. If the origin of the spatial coordinates is chosen at the center of gravity, the displacements of a point located at the solid surface Γ_s, $\boldsymbol{d}^c = (d_1, d_2)$, are related to the displacements of the center of gravity, $\boldsymbol{\delta} = (\delta_1, \delta_2)$, by $\boldsymbol{d}^c = \boldsymbol{\delta} + \boldsymbol{R}_c(\theta)\boldsymbol{x}^c$, where $\boldsymbol{x}^c = (x_1^c, x_2^c)$ denotes the surface nodes coordinates, and $\boldsymbol{R}_c(\theta)$ is a matrix that explicitly depends on the rotation angle θ

$$\boldsymbol{R}_c(\theta) = \begin{pmatrix} \cos\theta - 1 & -\sin\theta \\ \sin\theta & \cos\theta - 1 \end{pmatrix}.$$

By time differentiation it is possible to relate the velocity and the acceleration of the surface points, $\boldsymbol{v}^c$ and $\boldsymbol{a}^c$, to their counterparts $\boldsymbol{\nu}$ and $\boldsymbol{\alpha}$ defined at the center of gravity

$$\begin{aligned} \boldsymbol{v}^c &= \boldsymbol{T}_c(\theta)\ \boldsymbol{\nu} \\ \boldsymbol{a}^c &= \boldsymbol{T}_c(\theta)\ \boldsymbol{\alpha} + \hat{\boldsymbol{T}}_c(\theta)\ \boldsymbol{\nu}^2 \end{aligned} \tag{6}$$

where matrices

$$\boldsymbol{T}_c(\theta) = \begin{pmatrix} 1 & 0 & -L_2^c(\theta) \\ 0 & 1 & L_1^c(\theta) \end{pmatrix} \quad \text{and} \quad \hat{\boldsymbol{T}}_c(\theta) = \begin{pmatrix} 0 & 0 & -L_1^c(\theta) \\ 0 & 0 & -L_2^c(\theta) \end{pmatrix},$$

contain the following angle dependent coefficients: $L_1^c(\theta) = x_1^c \cos\theta - x_2^c \sin\theta$, and $L_2^c(\theta) = x_1^c \sin\theta + x_2^c \cos\theta$. Notice that matrix $\hat{\boldsymbol{T}}_c$ has been introduced in order to develop properly the new formulation. However, the term $\hat{\boldsymbol{T}}_c(\theta)\ \boldsymbol{\nu}^2$ in (6), in fact, only contains the product of the vector $\{-L_1^c, -L_2^c\}^T$ times the scalar θ^2.

An equivalent relation between the dynamic fluid force acting at a point located on the solid surface, $\boldsymbol{f}^c$, and its counterpart at the center of gravity, $\boldsymbol{\varphi}^c$, can be determined

$$-\boldsymbol{T}_c^T(\theta)\boldsymbol{f}^c = \boldsymbol{\varphi}^c. \tag{7}$$

Relationships (6) and (7) are defined for each point on the rigid body surface. Velocities, accelerations and forces of fluid and rigid body do coincide on the interface because the fluid is viscous. Thus, the following assembled vectors, which are needed in Eqs. (3) and (4), are produced:

$$\boldsymbol{v}^s = \left\{ \begin{array}{c} \vdots \\ \boldsymbol{v}^c \\ \vdots \end{array} \right\} = \left(\begin{array}{c} \vdots \\ \boldsymbol{T}_c(\theta) \\ \vdots \end{array} \right) \boldsymbol{\nu} = \boldsymbol{T}(\theta)\ \boldsymbol{\nu}, \tag{8}$$

$$\boldsymbol{a}^s = \left\{ \begin{array}{c} \vdots \\ \boldsymbol{a}^c \\ \vdots \end{array} \right\} = \left(\begin{array}{c} \vdots \\ \boldsymbol{T}_c(\theta) \\ \vdots \end{array} \right) \boldsymbol{\alpha} + \left(\begin{array}{c} \vdots \\ \hat{\boldsymbol{T}}_c(\theta) \\ \vdots \end{array} \right) \boldsymbol{\nu}^2 = \boldsymbol{T}(\theta)\ \boldsymbol{\alpha} + \hat{\boldsymbol{T}}(\theta)\ \boldsymbol{\nu}^2, \tag{9}$$

$$\begin{aligned} -\boldsymbol{T}^T(\theta)\ \boldsymbol{f}^s &= -\left(\ldots \quad \boldsymbol{T}_c^T(\theta) \quad \ldots \right) \left\{ \begin{array}{c} \vdots \\ \boldsymbol{f}^c \\ \vdots \end{array} \right\} = -\sum_c \boldsymbol{T}_c^T(\theta)\ \boldsymbol{f}^c \\ &= \sum_c \boldsymbol{\varphi}^c = \boldsymbol{\varphi}. \end{aligned} \tag{10}$$

These expressions are the *compatibility equations*. They relate the variables defined at a node of the fluid boundary with those defined at the center of gravity. Notice that the last equation is in fact a statement of equilibrium in the solid. It states that the total force and momentum acting at the center of gravity are the resultant of all the actions exercised on the solid boundary. $\boldsymbol{T}(\theta)$ and $\hat{\boldsymbol{T}}(\theta)$ are the *assembled transformation matrices*. They explicitly depend on the rotation angle θ, i.e. Eqs. (8), (9), and (10) are nonlinear. It has to be noted that the transformation matrices are rectangular and of order $N_S \times N_G$, where N_S is the number of unknowns on the rigid body surface and N_G is the number of unknowns defined at the center of gravity ($N_G \leq 3$).

2.4 Mesh motion description

Since the only moving boundary considered here is the rigid body surface, the mesh motion is defined as follows: *1.*- a Lagrangian description is imposed on the rigid body surface in the sense that at the fluid/solid interface the nodes of the fluid mesh are constrained to remain attached to the solid nodes during the whole calculation. The mesh velocity of the fluid nodes at the interface is imposed equal to the velocity of the corresponding fluid/solid nodes: $\hat{\boldsymbol{v}} = \boldsymbol{v}^s = \boldsymbol{T}(\theta)\ \boldsymbol{\nu}$; *2.*- in the outer part of the hydrodynamic domain an Eulerian description is imposed by stating: $\hat{\boldsymbol{v}} = \boldsymbol{0}$; and *3.*- in an area around the rigid body the mesh velocity decreases along with the distance to the rigid body surface according to a prescribed law, see [15] for details.

Note that, if a free surface exists, a Lagrangian description will be imposed on the nodes belonging to it, so that the computational mesh follows the motion of the fluid particles. Consequently, the algorithm for computing the mesh motion has to be changed accordingly. However, this change will only affect the mesh motion algorithm, and not to the general formulation of the problem.

3 PROPOSED NONLINEAR ALGORITHM

3.1 General formulation

In order to simplify the notation, the explicit dependence on the rotation angle will be dropped in the rest of the present paper. The general formulation for the fluid–rigid body interaction problem can be derived after substitution of the compatibility conditions (8) and (9) into Eq. (3), where the component related to the prescribed Dirichlet values is omitted. This yields the following system of differential equations,

$$\begin{aligned}&\begin{pmatrix} \boldsymbol{M}^{ff} & \boldsymbol{M}^{fs} \\ \boldsymbol{M}^{sf} & \boldsymbol{M}^{ss} \end{pmatrix} \begin{Bmatrix} \boldsymbol{a}^f \\ \boldsymbol{T}\,\boldsymbol{\alpha} + \hat{\boldsymbol{T}}\,\boldsymbol{\nu}^2 \end{Bmatrix} + \begin{pmatrix} \boldsymbol{K}^{ff} & \boldsymbol{K}^{fs} \\ \boldsymbol{K}^{sf} & \boldsymbol{K}^{ss} \end{pmatrix} \begin{Bmatrix} \boldsymbol{v}^f \\ \boldsymbol{T}\,\boldsymbol{\nu} \end{Bmatrix} \\ &+ \begin{Bmatrix} \boldsymbol{\eta}^f \\ \boldsymbol{\eta}^s \end{Bmatrix} - \begin{pmatrix} \boldsymbol{G}^f \\ \boldsymbol{G}^s \end{pmatrix} \boldsymbol{p} = \begin{Bmatrix} \tilde{\boldsymbol{f}}^f \\ \boldsymbol{f}^s \end{Bmatrix} - \begin{pmatrix} \boldsymbol{M}^{fd} \\ \boldsymbol{M}^{sd} \end{pmatrix} \tilde{\boldsymbol{a}}^d - \begin{pmatrix} \boldsymbol{K}^{fd} \\ \boldsymbol{K}^{sd} \end{pmatrix} \tilde{\boldsymbol{v}}^d. \end{aligned} \tag{11}$$

From the previous equation, an expression for the forces acting on the rigid body surface, $\boldsymbol{f}^s$, is obtained. Using this expression of $\boldsymbol{f}^s$ and Eq. (10), the rigid body equilibrium equation (5) can be rewritten as,

$$\begin{aligned}\boldsymbol{\mathcal{M}}^*\boldsymbol{\alpha} + \boldsymbol{\mathcal{C}}^*\boldsymbol{\nu} + \boldsymbol{\mathcal{K}}\boldsymbol{\delta} = -\boldsymbol{T}^T \Bigg[&\begin{pmatrix} \boldsymbol{M}^{sf} & \boldsymbol{M}^{ss} & \boldsymbol{M}^{sd} \end{pmatrix} \begin{Bmatrix} \boldsymbol{a}^f \\ \hat{\boldsymbol{T}}\,\boldsymbol{\nu}^2 \\ \tilde{\boldsymbol{a}}^d \end{Bmatrix} \\ &+ \begin{pmatrix} \boldsymbol{K}^{sf} & \boldsymbol{K}^{sd} & \boldsymbol{K}^{ss} \end{pmatrix} \begin{Bmatrix} \boldsymbol{v}^f \\ \boldsymbol{0} \\ \tilde{\boldsymbol{v}}^d \end{Bmatrix} + \boldsymbol{\eta}^s - \boldsymbol{G}^s\boldsymbol{p} \Bigg], \end{aligned} \tag{12}$$

where we have introduced the modified mass and damping matrices

$$\begin{aligned}\boldsymbol{\mathcal{M}}^* &= \boldsymbol{\mathcal{M}} + \boldsymbol{T}^T\boldsymbol{M}^{ss}\boldsymbol{T}, \\ \boldsymbol{\mathcal{C}}^* &= \boldsymbol{\mathcal{C}} + \boldsymbol{T}^T\boldsymbol{K}^{ss}\boldsymbol{T}.\end{aligned}$$

It is important to notice that the order of the matrices $\boldsymbol{\mathcal{M}}^*$ and $\boldsymbol{\mathcal{C}}^*$ is $N_G \leq 3$ (the number of degrees of freedom of the rigid body). Also, these matrices are no longer diagonal, but they remain symmetric.

In conclusion, the fluid–rigid body interaction problem can be described by a system of ordinary differential equations composed by the first equation in (11), Eq. (12) and mass conservation, Eq. (4). Rearranging the first two equations into a single system, we obtain:

$$
\begin{aligned}
&\begin{pmatrix} \boldsymbol{M}^{ff} & \boldsymbol{M}^{fs}\,\boldsymbol{T} \\ \boldsymbol{T}^T\,\boldsymbol{M}^{sf} & \boldsymbol{\mathcal{M}}^* \end{pmatrix} \begin{Bmatrix} \boldsymbol{a}^f \\ \boldsymbol{\alpha} \end{Bmatrix} + \begin{pmatrix} \boldsymbol{K}^{ff} & \boldsymbol{K}^{fs}\,\boldsymbol{T} \\ \boldsymbol{T}^T\,\boldsymbol{K}^{sf} & \boldsymbol{\mathcal{C}}^* \end{pmatrix} \begin{Bmatrix} \boldsymbol{v}^f \\ \boldsymbol{\nu} \end{Bmatrix} \\
&+ \begin{pmatrix} \boldsymbol{0} & \boldsymbol{M}^{fs}\,\hat{\boldsymbol{T}} \\ \boldsymbol{0} & \boldsymbol{T}^T\boldsymbol{M}^{ss}\hat{\boldsymbol{T}} \end{pmatrix} \begin{Bmatrix} \boldsymbol{0} \\ \boldsymbol{\nu}^2 \end{Bmatrix} + \begin{pmatrix} \boldsymbol{0} & \boldsymbol{0} \\ \boldsymbol{0} & \boldsymbol{\mathcal{K}} \end{pmatrix} \begin{Bmatrix} \boldsymbol{0} \\ \boldsymbol{\delta} \end{Bmatrix} + \begin{Bmatrix} \boldsymbol{\eta}^f \\ \boldsymbol{T}^T\boldsymbol{\eta}^s \end{Bmatrix} - \begin{pmatrix} \boldsymbol{G}^f \\ \boldsymbol{T}^T\boldsymbol{G}^s \end{pmatrix} \boldsymbol{P} \\
&= \begin{Bmatrix} \tilde{\boldsymbol{f}}^f \\ \boldsymbol{0} \end{Bmatrix} - \begin{pmatrix} \boldsymbol{M}^{fd} \\ \boldsymbol{T}^T\boldsymbol{M}^{sd} \end{pmatrix} \tilde{\boldsymbol{a}}^d - \begin{pmatrix} \boldsymbol{K}^{fd} \\ \boldsymbol{T}^T\boldsymbol{K}^{sd} \end{pmatrix} \tilde{\boldsymbol{v}}^d
\end{aligned} \tag{13}
$$

and

$$
\begin{pmatrix} \boldsymbol{G}^{f^T} & \boldsymbol{G}^{s^T}\boldsymbol{T} \end{pmatrix} \begin{Bmatrix} \boldsymbol{v}^f \\ \boldsymbol{\nu} \end{Bmatrix} = -\boldsymbol{G}^{d^T}\tilde{\boldsymbol{v}}^d, \tag{14}
$$

where the velocity compatibility condition (8) has been also included in (14). It has to be noted that the mass, viscosity and divergence matrices depend on the rotation angle θ.

3.2 Fluid–rigid body interaction with translation only

As previously noted, if a certain degree of freedom of the rigid body is fixed, the compatibility and the assembled transformation matrices have to be regarded as a reduced system. In particular, if the fixed degree of freedom is the rigid body rotation, then the equation of motion (5) can be written as:

$$
\boldsymbol{\mathcal{M}}_{tt}\boldsymbol{\alpha}_t + \boldsymbol{\mathcal{C}}_{tt}\boldsymbol{\nu}_t + \boldsymbol{\mathcal{K}}_{tt}\boldsymbol{\delta}_t = \boldsymbol{\varphi}_t \tag{15}
$$

where subscript t means translation. Furthermore, the nodal transformation matrices in (6) and (7) do not depend anymore on the rotation angle θ. Their order is $N_G \leq 2$, and they are equal to identity and null matrices, respectively ($\boldsymbol{T}_c = \boldsymbol{I_d}$ and $\hat{\boldsymbol{T}}_c = \boldsymbol{0}$).

Therefore, the assembled transformation matrices are also constant coefficient matrices. In fact, matrix $\hat{\boldsymbol{T}}(\theta)$, see (9), is null and the compatibility conditions for velocity and acceleration are identical

$$
\boldsymbol{v}^s = \boldsymbol{T}_t\boldsymbol{\nu}_t \qquad \boldsymbol{a}^s = \boldsymbol{T}_t\boldsymbol{\alpha}_t \qquad -\boldsymbol{T}_t^T\boldsymbol{f}^s = \boldsymbol{\varphi}
$$

where matrix $\boldsymbol{T}_t$ is the assembled transformation matrix for translations, and it is composed by 2×2 identity matrices.

The fluid–rigid body interaction problem is now described by the following system of ordinary differential equations, which is similar to (13) and (14). $\boldsymbol{T}$ is replaced by $\boldsymbol{T}_t$ and the $\boldsymbol{\nu}^2$ term has disappeared.

$$
\begin{aligned}
&\begin{pmatrix} \boldsymbol{M}^{ff} & \boldsymbol{M}^{fs}\,\boldsymbol{T}_t \\ \boldsymbol{T}_t^T\,\boldsymbol{M}^{sf} & \boldsymbol{\mathcal{M}}^*_{tt} \end{pmatrix} \begin{Bmatrix} \boldsymbol{a}^f \\ \boldsymbol{\alpha}_t \end{Bmatrix} + \begin{pmatrix} \boldsymbol{K}^{ff} & \boldsymbol{K}^{fs}\,\boldsymbol{T}_t \\ \boldsymbol{T}_t^T\,\boldsymbol{K}^{sf} & \boldsymbol{\mathcal{C}}^*_{tt} \end{pmatrix} \begin{Bmatrix} \boldsymbol{v}^f \\ \boldsymbol{\nu}_t \end{Bmatrix} \\
&+ \begin{pmatrix} \boldsymbol{0} & \boldsymbol{0} \\ \boldsymbol{0} & \boldsymbol{\mathcal{K}}_{tt} \end{pmatrix} \begin{Bmatrix} \boldsymbol{0} \\ \boldsymbol{\delta} \end{Bmatrix} + \begin{Bmatrix} \boldsymbol{\eta}^f \\ \boldsymbol{T}_t^T\boldsymbol{\eta}^s \end{Bmatrix} - \begin{pmatrix} \boldsymbol{G}^f \\ \boldsymbol{T}_t^T\boldsymbol{G}^s \end{pmatrix} \boldsymbol{p} \\
&= \begin{Bmatrix} \tilde{\boldsymbol{f}}^f \\ \boldsymbol{0} \end{Bmatrix} - \begin{pmatrix} \boldsymbol{M}^{fd} \\ \boldsymbol{T}_t^T\boldsymbol{M}^{sd} \end{pmatrix} \tilde{\boldsymbol{a}}^d - \begin{pmatrix} \boldsymbol{K}^{fd} \\ \boldsymbol{T}_t^T\boldsymbol{K}^{sd} \end{pmatrix} \tilde{\boldsymbol{v}}^d \qquad (16)
\end{aligned}
$$

$$
\begin{pmatrix} \boldsymbol{G}^{f^T} & \boldsymbol{G}^{s^T}\boldsymbol{T}_t \end{pmatrix} \begin{Bmatrix} \boldsymbol{v}^f \\ \boldsymbol{\nu}_t \end{Bmatrix} = \boldsymbol{G}^{d^T}\tilde{\boldsymbol{v}}^d \qquad (17)
$$

where the modified mass and damping matrices for translation problems are:

$$
\begin{aligned}
\boldsymbol{\mathcal{M}}^*_{tt} &= \boldsymbol{\mathcal{M}}_{tt} + \boldsymbol{T}_t^T\boldsymbol{M}^{ss}\boldsymbol{T}_t, \\
\boldsymbol{\mathcal{C}}^*_{tt} &= \boldsymbol{\mathcal{C}}_{tt} + \boldsymbol{T}_t^T\boldsymbol{K}^{ss}\boldsymbol{T}_t.
\end{aligned}
$$

The time integration algorithm used in Eqs. (16) and (17) is standard in viscous incompressible fluid–structure interaction, see [2,9]. The basic characteristic of our treatment of problems with translations only is the particular computational implementation of Eqs. (16) and (17). This implementation is based on a proper interpretation of three kinds of operations that appear very often in (16) and (17). Such operations are classified as follows: *1.*- to premultiply a matrix or a vector by the $\boldsymbol{T}_t^T$ matrix, *2.*- to postmultiply a matrix or a vector by the $\boldsymbol{T}_t$ matrix and *3.*- to premultiply a matrix by $\boldsymbol{T}_t^T$ and then postmultiply the result by the $\boldsymbol{T}_t$ matrix.

To this end, consider a general block square matrix $\boldsymbol{A}_{(n\times n)}$ composed of 2×2 boxes, $\boldsymbol{A}_{ij} \quad i,j = 1,\ldots,n$. Since matrix $\boldsymbol{T}_t$ is also composed of $\boldsymbol{T}_c$ matrices of order 2×2 (recall that $\boldsymbol{T}_c = \boldsymbol{I_d}$), then

$$
\begin{aligned}
\boldsymbol{T}_t^T\,\boldsymbol{A}\,\boldsymbol{T}_t &= \begin{pmatrix} \boldsymbol{I_d} & \boldsymbol{I_d} & \ldots & \boldsymbol{I_d} \end{pmatrix} \begin{pmatrix} \boldsymbol{A}_{11} & \boldsymbol{A}_{12} & \ldots & \boldsymbol{A}_{1n} \\ \boldsymbol{A}_{21} & \boldsymbol{A}_{22} & \ldots & \boldsymbol{A}_{2n} \\ \vdots & \ldots & \ddots & \vdots \\ \boldsymbol{A}_{n1} & \boldsymbol{A}_{n2} & \ldots & \boldsymbol{A}_{nn} \end{pmatrix} \begin{pmatrix} \boldsymbol{I_d} \\ \boldsymbol{I_d} \\ \vdots \\ \boldsymbol{I_d} \end{pmatrix} \\
&= \begin{pmatrix} \boldsymbol{I_d} & \boldsymbol{I_d} & \ldots & \boldsymbol{I_d} \end{pmatrix} \begin{pmatrix} \sum_{j=1}^{n} \boldsymbol{A}_{1j} \\ \sum_{j=1}^{n} \boldsymbol{A}_{2j} \\ \vdots \\ \sum_{j=1}^{n} \boldsymbol{A}_{nj} \end{pmatrix} \\
&= \sum_{i=1}^{n} \left(\sum_{j=1}^{n} \boldsymbol{A}_{ij} \right).
\end{aligned}
$$

Therefore, this operation of pre- and post-multiplication is equivalent to add all the rows and columns corresponding to nodes on the rigid body surface. Similarly, to premultiply by the $\boldsymbol{T}_t^T$ matrix amounts to adding all the rows of $\boldsymbol{A}$, and postmultiply by the $\boldsymbol{T}_t$ matrix is equivalent to adding all the columns of $\boldsymbol{A}$. Hence, the implementation of the above three kinds of operation is extremely easy. It is equivalent to assigne the same equation to each degree of fredom defined on each node on the rigid body surface. In this case, the assembly process will automatically do all the work.

3.3 Nonlinear algorithm for interactions with rotations

As will become apparent from the developments in Section 3.4, the analysis of fluid–rigid body interaction problems with rotations, which corresponds to the numerical resolution of Eqs. (13) and (14), will involve the solution of a nonlinear system of the form

$$\begin{pmatrix} \boldsymbol{B}_{11} & \boldsymbol{b}_{12}(\theta) \\ \boldsymbol{b}_{21}^T(\theta) & b_{22}(\theta) \end{pmatrix} \begin{Bmatrix} \boldsymbol{x}_1 \\ \theta \end{Bmatrix} = \begin{Bmatrix} \boldsymbol{r}_1(\boldsymbol{x}_1, \theta) \\ r_2(\boldsymbol{x}_1, \theta) \end{Bmatrix} \tag{18}$$

where $\boldsymbol{x}_1$ is the vector associated with the nodal unknowns in the whole fluid domain including the translation motion of the solid, while θ represents the unknown associated with the angular motion of the solid. The basic idea of the algorithm proposed here relies on the following considerations: *1.-* the basic nonlinear equation in (18) is the scalar equation corresponding to rotation angle θ, and *2.-* the $\boldsymbol{B}_{11}$ matrix, which does not depend on the rotation angle, is well approximated by its lumped form [7,9,13,14]. The rotation angle θ can be written, using the second equation of (18), as

$$\theta = \frac{1}{b_{22}(\theta)} \Big[\, r_2(\boldsymbol{x}_1, \theta) - \boldsymbol{b}_{21}^T(\theta) \; \boldsymbol{x}_1 \, \Big] \tag{19}$$

then, substituting in the first equation of (18), one obtains,

$$\Big[\, \boldsymbol{B}_{11} - \frac{\boldsymbol{b}_{12}(\theta) \;\; \boldsymbol{b}_{21}^T(\theta)}{b_{22}(\theta)} \, \Big] \; \boldsymbol{x}_1 = \boldsymbol{r}_1(\boldsymbol{x}_1, \theta) - \frac{r_2(\boldsymbol{x}_1, \theta)}{b_{22}(\theta)} \boldsymbol{b}_{12}(\theta). \tag{20}$$

Note that, in the previous equation, the matrix on the left hand side does not depend on $\boldsymbol{x}_1$. Thus, the left hand side in (20) is linear on $\boldsymbol{x}_1$. In fact, a similar structure is also encountered in the algorithm used for fluid and fluid–structure interaction problems in [2,9] (i.e. a system of equations with a linear left hand side and a nonlinear right hand side). Our goal here is to obtain an algorithm with an equivalent accuracy and efficiency to the one proposed in

[2,9], but dealing now with the extra nonlinearities due to rotations. Therefore, if it is possible to invert efficiently the matrix in (20), the resolution of (18) only incorporates an extra *scalar* nonlinear equation, (19), which can be solved efficiently.

The system matrix in (20) can be inverted via the Sherman and Morrison lemma [4] giving

$$\left[\boldsymbol{B}_{11} - \frac{\boldsymbol{b}_{12}(\theta)\ \boldsymbol{b}_{21}^T(\theta)}{b_{22}(\theta)}\right]^{-1} = \left[\boldsymbol{B}_{11}^{-1} - \frac{1}{\sigma}\boldsymbol{B}_{11}^{-1}\frac{\boldsymbol{b}_{21}(\theta)\ \boldsymbol{b}_{21}^T(\theta)}{b_{22}(\theta)}\boldsymbol{B}_{11}^{-1}\ \right]$$

where $\boldsymbol{B}_{11}^{-1}$ must exits and the condition $\sigma = 1 + \boldsymbol{b}_{21}^T(\theta)\ \boldsymbol{B}_{11}^{-1}\,\boldsymbol{b}_{21}(\theta) \neq 0$ must hold.

Under these conditions an algorithm can be devised which uses the same simplification as the one proposed in [2,9] (i.e. $\boldsymbol{B}_{11}$ is well approximated by its lumped form, $\boldsymbol{B}_{11}^{\text{Lump}}$). Then, the solution of (20) is

$$\begin{aligned}\boldsymbol{x}_1 = &\left[\left(\boldsymbol{B}_{11}^{\text{Lump}}\right)^{-1} - \frac{1}{\sigma}\left(\boldsymbol{B}_{11}^{\text{Lump}}\right)^{-1}\ \frac{\boldsymbol{b}_{21}(\theta)\ \boldsymbol{b}_{21}^T(\theta)}{b_{22}(\theta)}\left(\boldsymbol{B}_{11}^{\text{Lump}}\right)^{-1}\ \right] \\ &\left[\boldsymbol{r}_1(\boldsymbol{x}_1,\theta) - \frac{r_2(\boldsymbol{x}_1,\theta)}{b_{22}(\theta)}\boldsymbol{b}_{12}(\theta)\right]\end{aligned}$$

where, from the computational point of view, only *vector-vector* and *vector-scalar* products are required. This is also valid for the computation of σ.

It is important to notice that this algorithm can be easily extended to problems with several rigid bodies. In this case, the scalar equation containing the rotation angle becomes a linear system with as many unknowns as rigid bodies. Consistently, the σ constant becomes a matrix of the same order.

3.4 Fluid–rigid body interaction with rotations

In order to uncouple the translation motion of the rigid body from its rotational motion, the local matrices in (6) and (7) are separated in two parts,

$$\boldsymbol{T}_c = \begin{pmatrix} 1 & 0 & -L_2^c \\ 0 & 1 & L_1^c \end{pmatrix} = (\,\boldsymbol{T}_{ct}\ \ \boldsymbol{t}_{cr}\,) \ \text{ and } \ \hat{\boldsymbol{T}}_c = \begin{pmatrix} 0 & 0 & -L_1^c \\ 0 & 0 & -L_2^c \end{pmatrix} = (\,\boldsymbol{0}\ \ \hat{\boldsymbol{t}}_{cr}\,)$$

where the subscript $(_t)$ means translations, the subscript $(_r)$ means rotations. Note that $\boldsymbol{T}_{ct}$ is the nodal transformation matrix extensively used in section

3.2. We have also introduced the following vectors

$$\boldsymbol{t}_{cr} = \left\{ \begin{array}{c} -L_2^c \\ L_1^c \end{array} \right\} \qquad \text{and} \qquad \hat{\boldsymbol{t}}_{cr} = \left\{ \begin{array}{c} -L_1^c \\ -L_2^c \end{array} \right\}$$

Consequently, the compatibility conditions (8-10) can be written as:

$$\boldsymbol{v}^s = \left\{ \begin{array}{c} \vdots \\ \boldsymbol{v}^c \\ \vdots \end{array} \right\} = \left(\begin{array}{cc} \vdots & \vdots \\ \boldsymbol{T}_{ct} & \boldsymbol{t}_{cr} \\ \vdots & \vdots \end{array} \right) \boldsymbol{\nu} = \left(\boldsymbol{T}_t \quad \boldsymbol{t}_r \right) \boldsymbol{\nu} \tag{21}$$

$$\begin{aligned} \boldsymbol{a}^s = \left\{ \begin{array}{c} \vdots \\ \boldsymbol{a}^c \\ \vdots \end{array} \right\} &= \left(\begin{array}{cc} \vdots & \vdots \\ \boldsymbol{T}_{ct} & \boldsymbol{t}_{cr} \\ \vdots & \vdots \end{array} \right) \boldsymbol{\alpha} + \left(\begin{array}{cc} \vdots & \vdots \\ \boldsymbol{0} & \hat{\boldsymbol{t}}_{cr} \\ \vdots & \vdots \end{array} \right) \boldsymbol{\nu}^2 \\ &= \left(\boldsymbol{T}_t \quad \boldsymbol{t}_r \right) \boldsymbol{\alpha} + \left(\boldsymbol{0} \quad \hat{\boldsymbol{t}}_r \right) \boldsymbol{\nu}^2 \end{aligned} \tag{22}$$

$$\begin{aligned} -\left(\begin{array}{c} \boldsymbol{T}_t^T \\ \boldsymbol{t}_r^T \end{array} \right) \boldsymbol{f}^s &= -\left(\begin{array}{ccc} \cdots & \boldsymbol{T}_{ct}^T & \cdots \\ \cdots & \boldsymbol{t}_{cr}^T & \cdots \end{array} \right) \left\{ \begin{array}{c} \vdots \\ \boldsymbol{f}^c \\ \vdots \end{array} \right\} = -\sum_c \boldsymbol{T}_c^T \boldsymbol{f}^c \\ &= \sum_c \boldsymbol{\varphi}^c = \boldsymbol{\varphi} \end{aligned} \tag{23}$$

The same decomposition is applied to the rigid body mass, damping and stiffness matrices

$$\boldsymbol{\mathcal{M}} = \left(\begin{array}{cc} \boldsymbol{\mathcal{M}}_{tt} & \\ & \mathcal{M}_{33} \end{array} \right) \ , \quad \boldsymbol{\mathcal{C}} = \left(\begin{array}{cc} \boldsymbol{\mathcal{C}}_{tt} & \\ & \mathcal{C}_{33} \end{array} \right) \ , \quad \boldsymbol{\mathcal{K}} = \left(\begin{array}{cc} \boldsymbol{\mathcal{K}}_{tt} & \\ & \mathcal{K}_{33} \end{array} \right) \tag{24}$$

where $\boldsymbol{\mathcal{M}}_{tt}$, $\boldsymbol{\mathcal{C}}_{tt}$ and $\boldsymbol{\mathcal{K}}_{tt}$ are the mass, damping and stiffness matrices used in (15) for the translation case, and the scalar variables $\mathcal{M}_{33}$, $\mathcal{C}_{33}$ and $\mathcal{K}_{33}$ contain the rigid body rotation parameters. The same decomposition is applied to the rigid body acceleration, velocity and displacement unknown vectors

$$\boldsymbol{\alpha} = \left\{ \begin{array}{c} \alpha_1 \\ \alpha_2 \\ \ddot{\theta} \end{array} \right\} = \left\{ \begin{array}{c} \boldsymbol{\alpha}_t \\ \ddot{\theta} \end{array} \right\} \ , \ \boldsymbol{\nu} = \left\{ \begin{array}{c} \nu_1 \\ \nu_2 \\ \dot{\theta} \end{array} \right\} = \left\{ \begin{array}{c} \boldsymbol{\nu}_t \\ \dot{\theta} \end{array} \right\} \ , \ \boldsymbol{\delta} = \left\{ \begin{array}{c} \delta_1 \\ \delta_2 \\ \theta \end{array} \right\} = \left\{ \begin{array}{c} \boldsymbol{\delta}_t \\ \theta \end{array} \right\} \tag{25}$$

Equations (21) to (25) must be introduced in the general expressions (13) and (14). Moreover, the equations associated to the fluid motion and the rigid body translation, see Eqs. (16) and (17) in section 3.2, are explicitly separated from the rigid body rotation equation. The objective of this decomposition is to identify, and then treat in a different manner, the terms associated with translations and those related to rotations. The following systems of ordinary

differential equations describe the fluid-rigid body interaction with rotations (see [15] for details)

$$\begin{aligned}
&\begin{pmatrix} \boldsymbol{M}_{tt} & \boldsymbol{m}_{tr} \\ \boldsymbol{m}_{tr}^T & m_{rr} \end{pmatrix} \begin{Bmatrix} \boldsymbol{a}_t \\ \ddot{\theta} \end{Bmatrix} + \begin{pmatrix} \boldsymbol{K}_{tt} & \boldsymbol{k}_{tr} \\ \boldsymbol{k}_{tr}^T & k_{rr} \end{pmatrix} \begin{Bmatrix} \boldsymbol{v}_t \\ \dot{\theta} \end{Bmatrix} \\
&+ \begin{pmatrix} \boldsymbol{0} & \hat{\boldsymbol{m}}_{tr} \\ \boldsymbol{0} & \hat{m}_{rr} \end{pmatrix} \begin{Bmatrix} \boldsymbol{0} \\ \dot{\theta}^2 \end{Bmatrix} + \begin{pmatrix} \hat{\boldsymbol{K}}_{tt} & \boldsymbol{0} \\ \boldsymbol{0} & \hat{k}_{rr} \end{pmatrix} \begin{Bmatrix} \boldsymbol{d}_t \\ \theta \end{Bmatrix} + \begin{Bmatrix} \boldsymbol{\eta}_t \\ \eta_r \end{Bmatrix} \\
&- \begin{pmatrix} \boldsymbol{G}_{tt} \\ \boldsymbol{g}_r^T \end{pmatrix} \boldsymbol{p} = \begin{Bmatrix} \boldsymbol{f}_t \\ 0 \end{Bmatrix} - \begin{pmatrix} \boldsymbol{M}_{tt}^d \\ \boldsymbol{m}_r^{d^T} \end{pmatrix} \tilde{\boldsymbol{a}}^d - \begin{pmatrix} \boldsymbol{K}_{tt}^d \\ \boldsymbol{k}_r^{d^T} \end{pmatrix} \tilde{\boldsymbol{v}}^d
\end{aligned} \tag{26}$$

and

$$\begin{pmatrix} \boldsymbol{G}_{tt}^T & \boldsymbol{g}_r \end{pmatrix} \begin{Bmatrix} \boldsymbol{v}_t \\ \dot{\theta} \end{Bmatrix} = -\boldsymbol{G}^{d^T} \tilde{\boldsymbol{v}}^d \tag{27}$$

where several matrices, vectors and scalars have been introduced:

$$\begin{aligned}
\boldsymbol{a}_t &\equiv \begin{Bmatrix} \boldsymbol{a}^f \\ \boldsymbol{\alpha}_t \end{Bmatrix} & \boldsymbol{v}_t &\equiv \begin{Bmatrix} \boldsymbol{v}^f \\ \boldsymbol{\nu}_t \end{Bmatrix} \\
\boldsymbol{d}_t &\equiv \begin{Bmatrix} \boldsymbol{0} \\ \boldsymbol{\delta} \end{Bmatrix} & \boldsymbol{f}_t &\equiv \begin{Bmatrix} \tilde{\boldsymbol{f}}^f \\ \boldsymbol{0} \end{Bmatrix} \\
\boldsymbol{M}_{tt} &\equiv \begin{pmatrix} \boldsymbol{M}^{ff} & \boldsymbol{M}^{fs}\,\boldsymbol{T}_t \\ \boldsymbol{T}_t^T\,\boldsymbol{M}^{sf} & \boldsymbol{\mathcal{M}}_{tt}^* \end{pmatrix} & \boldsymbol{M}_{tt}^d &\equiv \begin{pmatrix} \boldsymbol{M}^{fd} \\ \boldsymbol{T}_t^T \boldsymbol{M}^{sd} \end{pmatrix} \\
\boldsymbol{K}_{tt} &\equiv \begin{pmatrix} \boldsymbol{K}^{ff} & \boldsymbol{K}^{fs}\,\boldsymbol{T}_t \\ \boldsymbol{T}_t^T\,\boldsymbol{K}^{sf} & \boldsymbol{\mathcal{C}}_{\boldsymbol{tt}}^* \end{pmatrix} & \boldsymbol{K}_{tt}^d &\equiv \begin{pmatrix} \boldsymbol{K}^{fd} \\ \boldsymbol{T}_t^T \boldsymbol{K}^{sd} \end{pmatrix} \\
\hat{\boldsymbol{K}}_{tt} &\equiv \begin{pmatrix} \boldsymbol{0} & \boldsymbol{0} \\ \boldsymbol{0} & \boldsymbol{\mathcal{K}}_{tt} \end{pmatrix} & \boldsymbol{G}_{tt} &\equiv \begin{pmatrix} \boldsymbol{G}^f \\ \boldsymbol{T}_t^T\,\boldsymbol{G}^s \end{pmatrix} \\
\boldsymbol{\eta}_t &\equiv \begin{Bmatrix} \boldsymbol{\eta}^f \\ \boldsymbol{T}_t^T\,\boldsymbol{\eta}^s \end{Bmatrix} & \boldsymbol{g}_r^T &\equiv \{\, \boldsymbol{t}_r^T \boldsymbol{G}^s \,\} \\
\boldsymbol{m}_{tr} &\equiv \begin{Bmatrix} \boldsymbol{M}^{fs}\,\boldsymbol{t}_r \\ \boldsymbol{T}_t^T \boldsymbol{M}^{ss} \boldsymbol{t}_r \end{Bmatrix} & \boldsymbol{m}_r^{d^T} &\equiv \boldsymbol{t}_r^T \boldsymbol{M}^{sd} \\
\boldsymbol{k}_{tr} &\equiv \begin{Bmatrix} \boldsymbol{K}^{fs}\,\boldsymbol{t}_r \\ \boldsymbol{T}_t^T \boldsymbol{K}^{ss} \boldsymbol{t}_r \end{Bmatrix} & \boldsymbol{k}_r^{d^T} &\equiv \boldsymbol{t}_r^t\;\boldsymbol{K}^{sd} \\
\hat{\boldsymbol{m}}_{tr} &\equiv \begin{Bmatrix} \boldsymbol{M}^{fs}\,\hat{\boldsymbol{t}}_r \\ \boldsymbol{T}_t^T \boldsymbol{M}^{ss}\,\hat{\boldsymbol{t}}_r \end{Bmatrix} & \eta_r &\equiv \boldsymbol{t}_r^T \boldsymbol{e} \\
m_{rr} &\equiv \mathcal{M}_{33} + \boldsymbol{t}_r^T\;\boldsymbol{M}^{ss}\;\boldsymbol{t}_r & \hat{m}_{rr} &\equiv \boldsymbol{t}_r^T\;\boldsymbol{M}^{ss}\;\hat{\boldsymbol{t}}_r \\
k_{rr} &\equiv \mathcal{C}_{33} + \boldsymbol{t}_r^T\;\boldsymbol{K}^{ss}\;\boldsymbol{t}_r & \hat{k}_{rr} &\equiv \mathcal{K}_{33}
\end{aligned}$$

Finally, note that: *1.*– at this point it is trivial to prove that, if the rigid body rotation is fixed (no rotations exist), Eqs. (16) and (17) are a particular case of (26) and (27); and *2.*– the generalized mass and fluid viscosity matrices in

(26) and (27) have the same structure as the matrix in Eq. (18). Therefore, the algorithm introduced in section 3.3 can be applied to this problem.

The details of the practical implementation of time integration algorithm are presented in an appendix.

4 NUMERICAL EXAMPLES

Two examples are presented in this section to illustrate the algorithms for fluid-rigid body interaction discussed in the present paper. In both cases, we have used an upwind Petrov-Galerkin [2] formulation for solving equations (26) and (27). Bilinear velocity constant pressure (`Q1P0`) elements were employed for the spatial discretization.

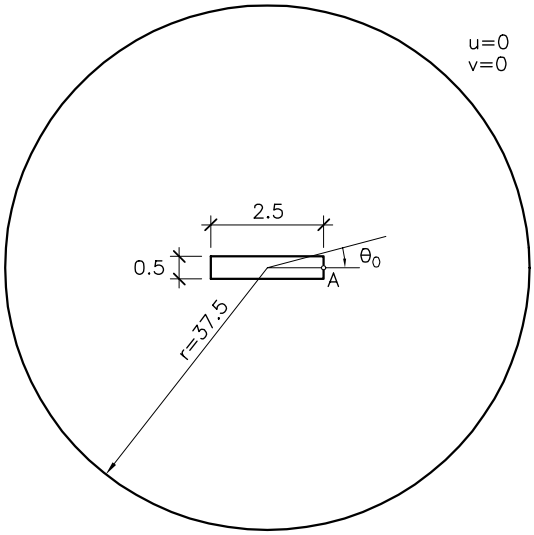

Fig. 2. Geometry and boundary conditions for the first example

In the first example, we analyze the attenuation of the rotational motion of a rectangular cylinder submerged in a viscous fluid (see Fig. 2). The structural damping is ignored in this case. Initially, the fluid and the rectangular cylinder are at rest. The cylinder is then released from an initial angular displacement $\theta_0 = 5^o$. The rigid body torsional frequency is taken as $\omega_r = \sqrt{k_r/I} = 0.266\, s^{-1}$. The problem is scaled using half of the rigid body base: $L = b/2 = 1.25$ as the characteristic length . The velocity scale is the maximum linear velocity of point A rotating without damping: $V = \theta_0\, \omega_r\, \sin(\omega_r T/2)\, L = 2.90245\, 10^{-2}$ (see Fig. 2). Since there is no damping in the system, the potential energy of the spring has to be absorbed by fluid forces. Therefore, the rotation amplitude of the rectangular cylinder has to decrease with both viscosity and time.

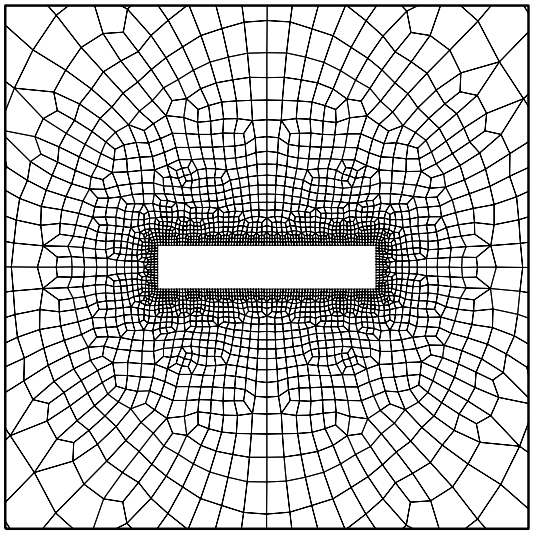

Fig. 3. Detail of the mesh for the first example

In order to analyze the rigid body motion dependence on the fluid viscosity three values of the kinematic viscosity, and hence three values of the Reynolds number, were used:

$$\begin{aligned} \nu = 0.01 \quad &\longrightarrow \quad R_e = 3.628 \\ \nu = 0.001 \quad &\longrightarrow \quad R_e = 36.28 \\ \nu = 0.0001 \quad &\longrightarrow \quad R_e = 362.8 \end{aligned}$$

The mesh employed consists of 3204 nodes and 3092 elements (see Fig. 3).

Figure 4 shows the evolution in time of the angular displacement, velocity and acceleration of the rigid body for the above values of the Reynolds number. The solid oscillates around its equilibrium position and the amplitude of the oscillatory motion decreases with time due to the effect of the hydrodynamic forces acting on the boundary of the solid. Note a strong amplitude attenuation for $R_e = 3.628$ ($\nu = 0.01$).

Figure 5 shows the streamlines for the two limit cases: $R_e = 3.628$ and $R_e = 362.8$. These results present a reasonable agreement with those obtained in [7] for translational motion: for high Reynolds numbers most of the shearing occurs in a small layer surrounding the rigid body and the vortices remain attached to the rigid body surface.

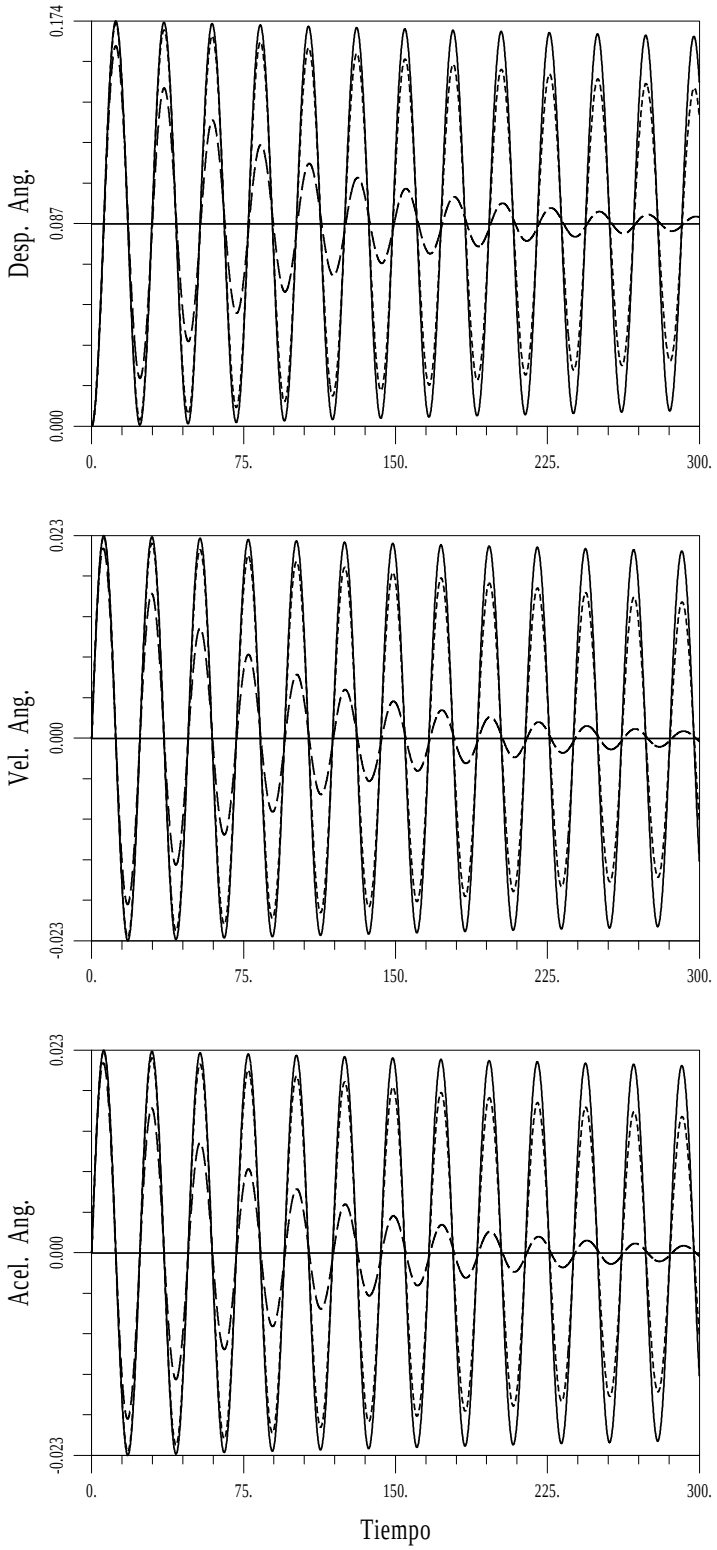

Fig. 4. Rigid body angular displacements: $R_e = 362.8$: ————; $R_e = 36.28$: – – – –; $R_e = 3.628$: — — —

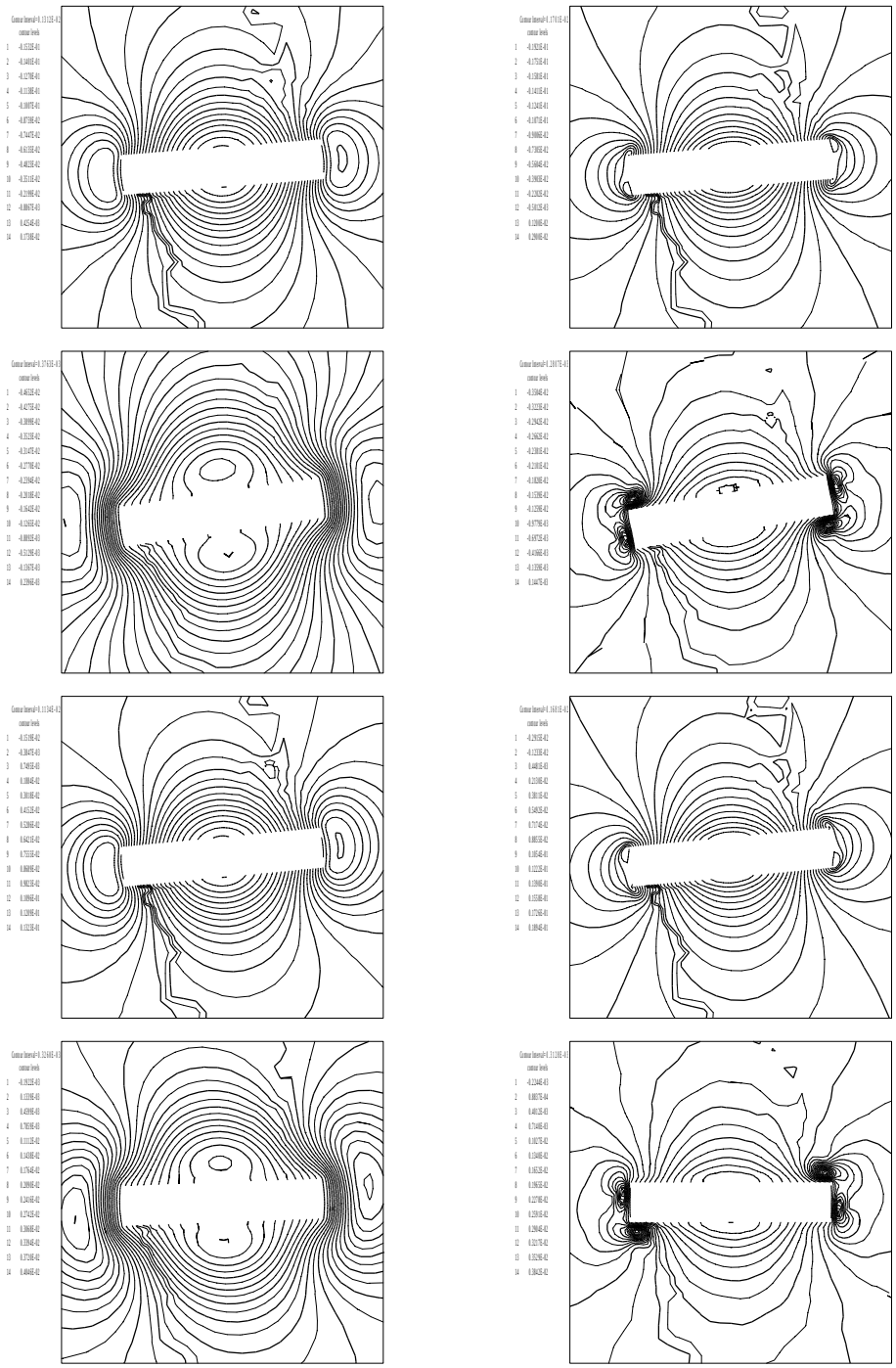

(a) **(b)**

Fig. 5. Streamlines for **(a)** $\nu = 0.01$ ($R_e = 3.628$) and **(b)** $\nu = 0.0001$ ($R_e = 362.8$). The snapshots correspond to $t = \pi/4$, $t = \pi/2$, $t = 3\pi/4$ and $t = 2\pi$

In the second example, the proposed formulation is applied to a fluid–rigid body interaction problem with cross-flow and rotational oscillations. Figure 6 shows the geometry of the problem and the applied boundary conditions. The computational mesh consists of 3204 nodes and 3092 elements (see Fig. 7). The non-dimensional parameters are obtained from the rigid body height and inflow velocity. For $R_e = 1000$ the non-dimensional rigid body parameters are:

$$m_t^* = 195.57 \qquad c_t^* = 0.0325 \qquad k_t^* = 0.7864$$
$$I^* = 105.94 \qquad c_r^* = 0.0 \qquad k_r^* = 17.05$$

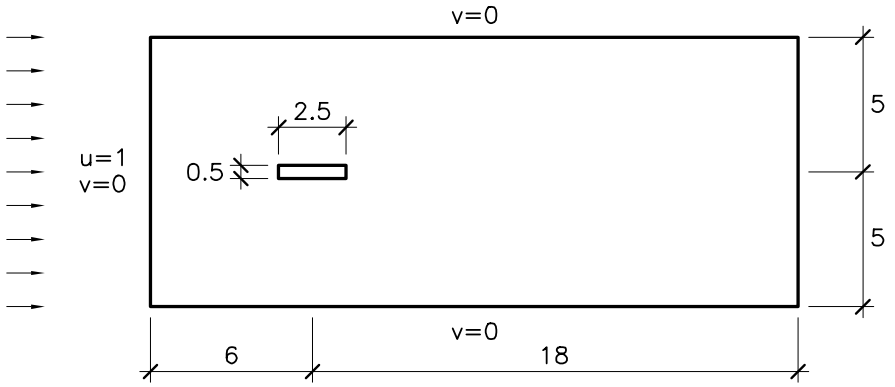

Fig. 6. Geometry and boundary conditions for the second example

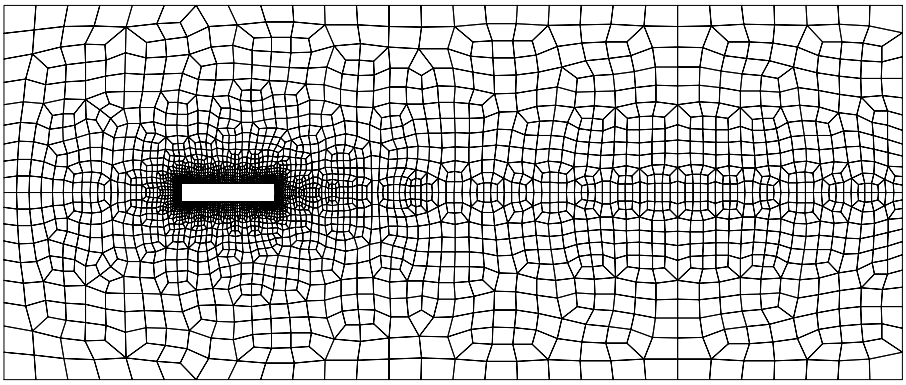

Fig. 7. Unstructured quadrilateral mesh for the second example

Figure 8 shows the vertical and rotational rigid body displacements, velocities and accelerations corresponding to $R_e = 1000$. As can be seen, after the initial transient, both motions only contain one main harmonic. In Figure 9 the stationary streamlines and the pressure field corresponding to the ultimate instants are presented.

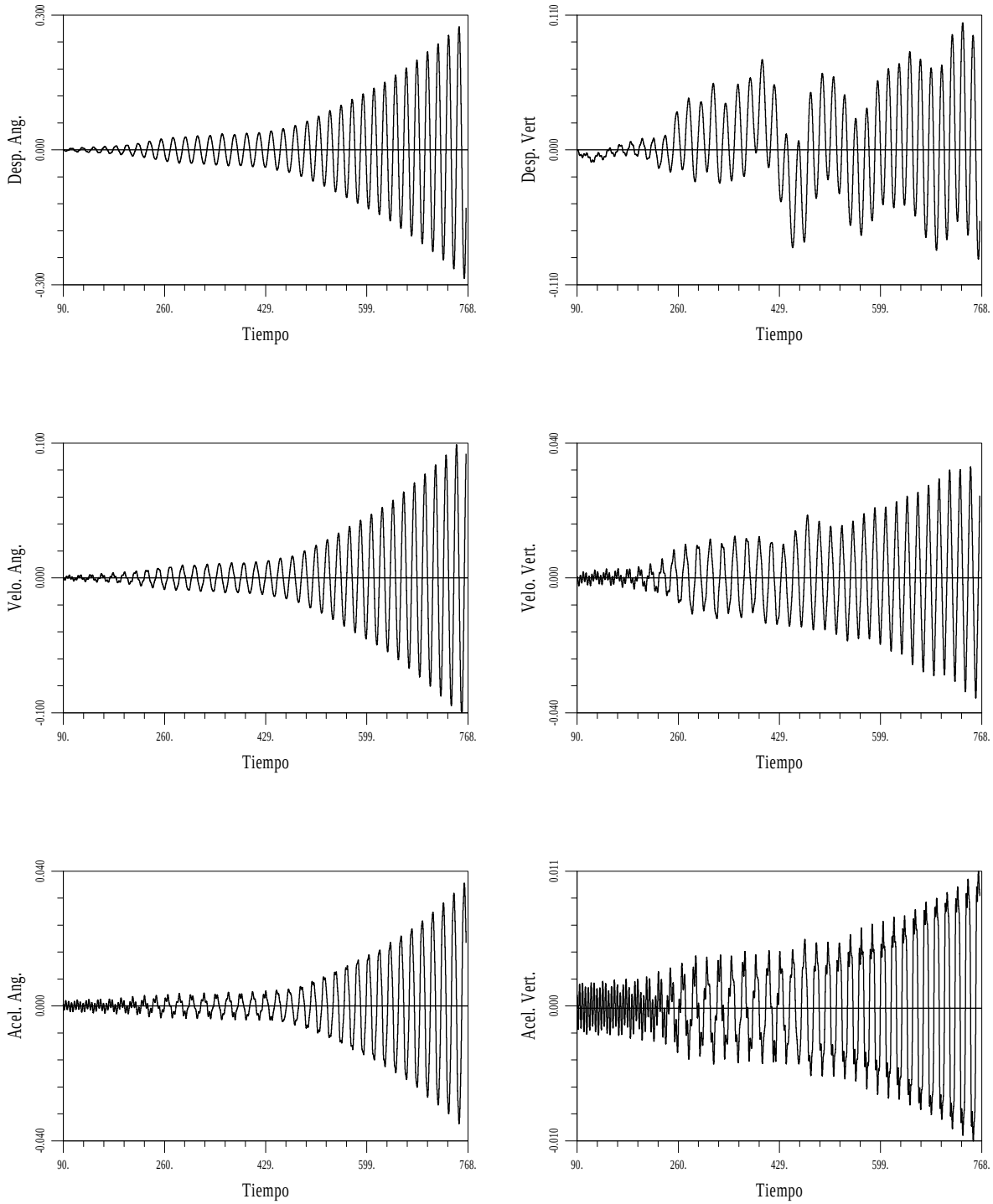

(a) **(b)**

Fig. 8. **(a)** Angular displacement and **(b)** vertical displacement of the rigid body

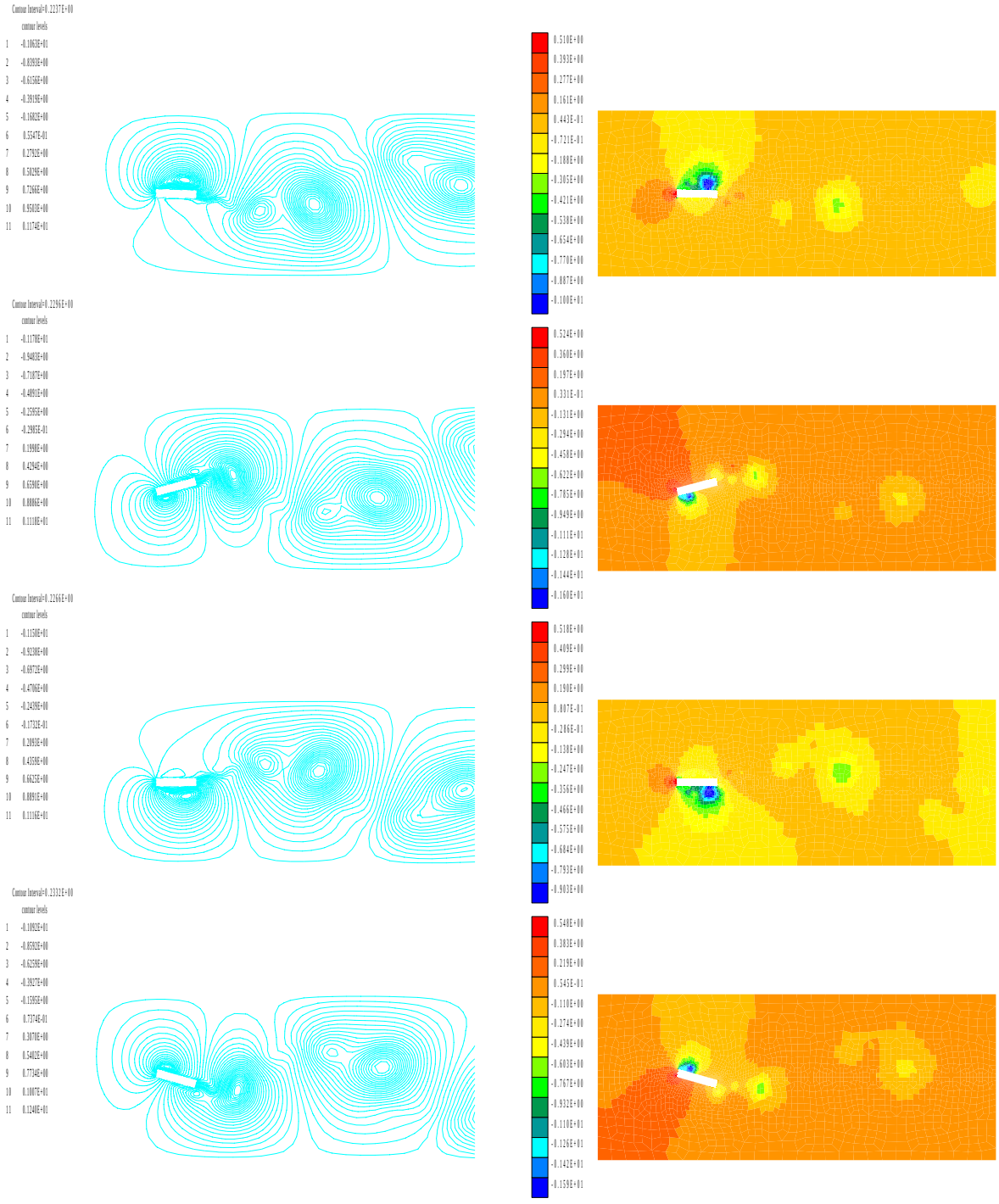

(a) **(b)**

Fig. 9. **(a)** Stationary streamlines and **(b)** pressure field around the rigid body

5 CONCLUSIONS

In this paper a new ALE algorithm for the numerical simulation of fluid–rigid body interaction problems has been developed. The basic characteristics of the proposed methodology are that *1.-* the equations governing the fluid motion and the rigid body translations are uncoupled from the scalar equation governing the rigid body rotation; and *2.-* a specific algorithm has been developed for efficiently solving the nonlinear system that appears when rotations of the rigid body are included. It is important to note that the resulting algorithm possesses the same structure as the standard predictor–multicorrector method used for the unsteady incompressible Navier–Stokes equations [2,7,9,14]. Furthermore, it maintains the same truncation error in time indicating that no loss in the time accuracy has resulted from the coupling between the fluid and a rigid solid. Finally, it is stressed that the present algorithm can be easily extended to deal with problems incorporating several rigid bodies.

6 APPENDIX: Time marching algorithm

In order to solve the systems of differential equations (26) and (27) a time discretization algorithm needs to be introduced. As already indicated, a nowadays standard time integration algorithm used in viscous incompressible fluid–structure interaction is employed, see [2,9]. In this predictor-corrector method [8], which belongs to the Newmark family, calculations start with the given initial data and the unknowns are then updated according to:

$$
\begin{aligned}
\boldsymbol{a}_t^{\nu+1} &= \boldsymbol{a}_t^{\nu} + \Delta \boldsymbol{a}_t^{\nu+1} & \ddot{\theta}^{\nu+1} &= \ddot{\theta}^{\nu} + \Delta \ddot{\theta}^{\nu+1} \\
\boldsymbol{v}_t^{\nu+1} &= \boldsymbol{v}_t^{\nu} + \gamma \Delta t \Delta \boldsymbol{a}_t^{\nu+1} & \dot{\theta}^{\nu+1} &= \dot{\theta}^{\nu} + \gamma \Delta t \Delta \ddot{\theta}^{\nu+1} \\
\boldsymbol{d}_t^{\nu+1} &= \boldsymbol{d}_t^{\nu} + \beta \Delta t^2 \Delta \boldsymbol{a}_t^{\nu+1} & \theta^{\nu+1} &= \theta^{\nu} + \beta \Delta t^2 \Delta \ddot{\theta}^{\nu+1} \\
\dot{\boldsymbol{p}}^{\nu+1} &= \dot{\boldsymbol{p}}^{\nu} + \Delta \dot{\boldsymbol{p}}^{\nu+1} & \boldsymbol{p}^{\nu+1} &= \boldsymbol{p}^{\nu} + \alpha \Delta t \Delta \dot{\boldsymbol{p}}^{\nu+1}
\end{aligned}
\tag{28}
$$

where the superscript ν is the iteration counter, and Δt is the time step. By introducing (28) into (26) and (27) the following system is obtained,

$$
\left.
\begin{aligned}
\begin{pmatrix} \boldsymbol{B} & \boldsymbol{c} \\ \boldsymbol{e}^T & s \end{pmatrix} \begin{Bmatrix} \Delta \boldsymbol{a}_t^{\nu+1} \\ \Delta \ddot{\theta}^{\nu+1} \end{Bmatrix} - \alpha \Delta t \begin{pmatrix} \boldsymbol{G}_{tt} \\ \boldsymbol{g}_r^T \end{pmatrix} \Delta \dot{\boldsymbol{p}}^{\nu+1} &= \begin{Bmatrix} \boldsymbol{r}_1 \\ r_2 \end{Bmatrix} \\
\gamma \Delta t \begin{pmatrix} \boldsymbol{G}_{tt}^T & \boldsymbol{g}_r \end{pmatrix} \begin{Bmatrix} \Delta \boldsymbol{a}_t^{\nu+1} \\ \Delta \ddot{\theta}^{\nu+1} \end{Bmatrix} &= -\boldsymbol{r}_p
\end{aligned}
\right\}
$$

where the following matrices, vectors an scalars have been defined

$$
\begin{aligned}
\boldsymbol{B} &\equiv \boldsymbol{M}_{tt} + \gamma\Delta t\ \boldsymbol{K}_{tt} + \beta\Delta t^2\,\hat{\boldsymbol{K}}_{tt} \\
\boldsymbol{c} &\equiv \boldsymbol{m}_{tr} + \gamma\Delta t\ \Big(\boldsymbol{k}_{tr} + 2\dot{\theta}^{\nu}\hat{\boldsymbol{m}}_{tr}\Big) + \gamma^2\Delta t^2\hat{\boldsymbol{m}}_{tr}(\ddot{\theta}^{\nu})^2 \\
\boldsymbol{e}^T &\equiv \boldsymbol{m}_{tr}^T + \gamma\Delta t\ \boldsymbol{k}_{tr}^T \\
s &\equiv m_{rr} + \gamma\Delta t\Big(k_{rr} + 2\dot{\theta}^{\nu}\hat{m}_{rr}\Big) + \beta\Delta t^2\hat{k}_{rr} + \gamma^2\Delta t^2\hat{m}_{rr}(\ddot{\theta}^{\nu})^2 \\
\boldsymbol{r}_1 &\equiv \boldsymbol{f}_t - \boldsymbol{M}_{tt}^d\tilde{\boldsymbol{a}}^d - \boldsymbol{K}_{tt}^d\tilde{\boldsymbol{v}}^d - \boldsymbol{M}_{tt}\boldsymbol{a}_t^{\nu} - \boldsymbol{K}_{tt}\boldsymbol{v}_t^{\nu} - \\
&\quad \hat{\boldsymbol{K}}_{tt}\boldsymbol{d}_t^{\nu} - \boldsymbol{m}_{tr}\ddot{\theta}^{\nu} - \boldsymbol{k}_{tr}\dot{\theta}^{\nu} - \hat{\boldsymbol{m}}_{tr}(\dot{\theta}^{\nu})^2 - \boldsymbol{\eta}_t^{\nu} + \boldsymbol{G}_{tt}\boldsymbol{p}^{\nu} \\
r_2 &\equiv -\boldsymbol{m}_r^{d^T}\tilde{\boldsymbol{a}}^d - \boldsymbol{k}_r^{d^T}\tilde{\boldsymbol{v}}^d - m_{rr}\ddot{\theta}^{\nu} - k_{rr}\dot{\theta}^{\nu} - \hat{m}_{rr}(\dot{\theta}^{\nu})^2 - \hat{k}_{rr}\theta^{\nu} \\
&\quad -\boldsymbol{m}_{tr}^T\boldsymbol{a}_t^{\nu} - \boldsymbol{k}_{tr}^T\boldsymbol{v}_t^{\nu} - \eta_r^{\nu} + \boldsymbol{g}_r^T\boldsymbol{p}^{\nu} \\
\boldsymbol{r}_p &\equiv \begin{pmatrix} \boldsymbol{G}_{tt}^T & \boldsymbol{g}_r & \boldsymbol{G}^{d^T} \end{pmatrix} \begin{Bmatrix} \boldsymbol{v}_t^{\nu} \\ \dot{\theta}^{\nu} \\ \tilde{\boldsymbol{v}}^d \end{Bmatrix}
\end{aligned}
\tag{29}
$$

As in the standard method, the acceleration increments are decomposed in the form

$$
\begin{aligned}
\Delta\boldsymbol{a}_t^{\nu+1} &= \Delta\boldsymbol{a}_t + \Delta\boldsymbol{a}_t^* \\
\Delta\ddot{\theta}^{\nu+1} &= \Delta\ddot{\theta} + \Delta\ddot{\theta}^*
\end{aligned}
$$

where $\Delta\boldsymbol{a}_t$ and $\Delta\ddot{\theta}$ can be interpreted as the acceleration increments due to the increment of the time derivative of the pressure, while $\Delta\boldsymbol{a}_t^*$ and $\Delta\ddot{\theta}^*$ correspond to the increments due to the residual of the previous iteration. After some matrix manipulation, see [15] for details, it can be proved that three systems must be solved at each time step. The first one reads

$$
\begin{pmatrix} \boldsymbol{B} & \boldsymbol{c} \\ \boldsymbol{e}^T & s \end{pmatrix} \begin{Bmatrix} \Delta\boldsymbol{a}_t^* \\ \Delta\ddot{\theta}^* \end{Bmatrix} = \begin{Bmatrix} \boldsymbol{r}_1 \\ r_2 \end{Bmatrix} \tag{30}
$$

Then, once $\Delta\boldsymbol{a}_t^*$ and $\Delta\ddot{\theta}^*$ are obtained, we have to solve for the increments of the temporal derivative of the pressure

$$
\begin{aligned}
&\left\{\frac{1}{s}\boldsymbol{g}_r\boldsymbol{g}_r^T + \left[\boldsymbol{G}_{tt}^T - \frac{1}{s}\boldsymbol{g}_r\boldsymbol{e}^T\right]\ \left[\boldsymbol{B} - \frac{1}{s}\boldsymbol{c}\boldsymbol{e}^T\right]^{-1}\left[\boldsymbol{G}_{tt} - \frac{1}{s}\boldsymbol{c}\boldsymbol{g}_r^T\right]\right\}\Delta\dot{\boldsymbol{p}}^{\nu+1} \\
&\qquad = \frac{-1}{\alpha\gamma\Delta t^2}\boldsymbol{r}_p^*
\end{aligned}
\tag{31}
$$

where the following residual for the pressure has been introduced:

$$\boldsymbol{r}_p^* = \boldsymbol{r}_p + \gamma \Delta t \, (\, \boldsymbol{G}_{tt} \quad \boldsymbol{g}_r \,) \left\{ \begin{array}{c} \Delta \boldsymbol{a}_t^* \\ \Delta \ddot{\theta}^* \end{array} \right\}$$

Third, and finally, we have to solve the system

$$\left(\begin{array}{cc} \boldsymbol{B} & \boldsymbol{c} \\ \boldsymbol{e}^T & s \end{array} \right) \left\{ \begin{array}{c} \Delta \boldsymbol{a}_t^* \\ \Delta \ddot{\theta}^* \end{array} \right\} = \left\{ \begin{array}{c} \boldsymbol{r}_{a_t} \\ r_\theta \end{array} \right\} \tag{32}$$

where the following residuals have been introduced for the accelerations

$$\begin{aligned} \boldsymbol{r}_{a_t} &\equiv -\alpha \Delta t \left[\frac{1}{s} \boldsymbol{c} \boldsymbol{g}_r^T - \boldsymbol{G}_{tt}^T \right] \Delta \dot{\boldsymbol{p}}^{\nu+1} \\ r_\theta &\equiv -\alpha \Delta t \boldsymbol{g}_r^T \Delta \dot{\boldsymbol{p}}^{\nu+1} \end{aligned}$$

At this point, several aspects of the time-stepping procedure should be highlighted. If a first order approximation is chosen in (29), then $\boldsymbol{B} = \boldsymbol{M}_{tt}$. Hence, matrix $\boldsymbol{B}$ can be substituted by the lumped approximation of $\boldsymbol{M}_{tt}$, but more importantly, one has $\boldsymbol{c} = \boldsymbol{e}^T$ and the matrices in Eqs. (30), (31) and (32) are symmetric matrices.

Moreover, the systems of equations that must be solved in (30) and (32) have the same structure as the one in (18). Therefore, the solution technique presented in section 3.3 can be applied. That is, the Sherman and Morrison lemma [4] can also be applied to invert the matrix $[\, \boldsymbol{B} - \frac{1}{s} \boldsymbol{c} \, \boldsymbol{e}^T \,]$ in system (31). Actually, system (31) can be rewritten as

$$\begin{aligned} &\left\{ \frac{1}{s} \boldsymbol{g}_r \boldsymbol{g}_r^T + \left[\boldsymbol{G}_{tt}^T - \frac{1}{s} \boldsymbol{g}_r \boldsymbol{e}^T \right] \left[\boldsymbol{B}^{-1} - \hat{\boldsymbol{B}}^{-1} \right] \left[\boldsymbol{G}_{tt} - \frac{1}{s} \boldsymbol{c} \boldsymbol{g}_r^T \right] \right\} \Delta \dot{\boldsymbol{p}}^{\nu+1} \\ &\qquad = \frac{-1}{\alpha \gamma \Delta t^2} \boldsymbol{r}_p^* \end{aligned}$$

where we have defined

$$\hat{\boldsymbol{B}}^{-1} = \frac{1}{\sigma} \boldsymbol{B}^{-1} \frac{1}{s} \boldsymbol{c} \, \boldsymbol{e}^T \boldsymbol{B}^{-1}$$

References

[1] T. Belytschko, J.M. Kennedy, and D.F. Schoeberle, Quasi-Eulerian finite element formulation for fluid structure interaction, *ASME J. Pressure Vessel Technol.* **102** (1980) 62–69.

[2] A.N. Brooks and T.J.R. Hughes, Streamline Upwind/Petrov Galerkin formulations for convection dominated flows with particular emphasis on the incompressible Navier Stokes equation, *Comput. Meths. Appl. Mech. Engrg.* **32** (1982) 199–259.

[3] F. Casadei and J.P. Halleux, An algorithm for permanent fluid-structure interaction in explicit transient analysis, *Comput. Meths. Appl. Mech. Engrg.* **128** (1995) 231–289.

[4] J.E. Dennis and J.J. Moré, Quasi–Newton methods, motivation and theory, *SIAM Rev.* **19** (1977) 46–89.

[5] J. Donea, S. Giuliani, and J.P. Halleux, An arbitrary Lagrangian-Eulerian finite element method for transient dynamic fluid–structure interactions, *Comput. Meths. Appl. Mech. Engrg.* **33** (1982) 689–723.

[6] H. Hirano, A. Maruoka and M. Kawahara, Finite element analysis of fluid–structure interaction problem and its application to wind resistance design of box girder bridges, in: M. Cecchi et al., eds., *Proceedings 9th International Conference on Finite Elements in Fluids* (Venecia, Italy, 1994) 235–244.

[7] A. Huerta and W.K. Liu, Viscous flow structure interaction, *ASME J. Pressure Vessel Technol.* **110** (1988) 15–21.

[8] T.J.R. Hughes, *The finite element method* (Prentice Hall, Englewood Cliffs, NJ, 1988).

[9] W.K. Liu and J. Gvildys, Fluid structure interaction of tanks with an eccentric core barrel, *Comput. Meths. Appl. Mech. Engrg.* **58** (1985) 51–77.

[10] W.K. Liu and D. Ma, Computer implementation aspects for fluid structure interaction problems, *Comput. Meths. Appl. Mech. Engrg.* **31** (1982) 129–148.

[11] S. Mittal and T.E. Tezduyar, A finite element study of incompressible flows past oscillating cylinders and aerofoils, *Comput. Meths. Appl. Mech. Engrg.* **95** (1992) 1073–1118.

[12] S. Mittal and T.E. Tezduyar, Massively parallel finite element computation of incompressible flows involving fluid–body interactions, *Comput. Meths. Appl. Mech. Engrg.* **112** (1994) 253–282.

[13] T. Nomura, ALE finite element computations of fluid–structure interaction problems, *Comput. Meths. Appl. Mech. Engrg.* **112** (1994) 291–308.

[14] T. Nomura and T.J.R. Hughes, An Arbitrary Lagrangian Eulerian finite element method for interaction of fluid and rigid body, *Comput. Meths. Appl. Mech. Engrg.* **95** (1992) 115–138.

[15] Sarrate, J. *Modelización numérica de la interacción fluido-sólido rígido: desarrollo de algoritmos, generación de mallas y adaptividad* (Doctoral Thesis, Universitat Politècnica de Catalunya, Barcelona, 1996).